Self-assembly and biological activities of ionic liquid crystals derived from aromatic amino acids

Manuel M. Neidhardt,[a] Katharina Schmitt,[a] Angelika Baro,[a] Carmen Schneider,[b] Ursula Bilitewski*[b] and Sabine Laschat[ID]*[a]

The self-assembly of amino acid-derived ionic liquid crystals (ILCs) into lamellar or micellar-like aggregates suggests that they might interact with biological membranes. To get some insight, guanidinium chlorides derived from natural L-amino acids phenylalanine (Phe), tyrosine (Tyr) and 3,4-dihydroxyphenylalanine (DOPA) were synthesized and mesomorphic properties investigated by polarizing optical microscopy (POM), differential scanning calorimetry (DSC) and X-ray diffraction (SAXS, WAXS). Mesophase types depended on the number of alkoxy side chains. Phe- and Tyr-based ILCs with one and two side chains, respectively, self-assembled into smectic A bilayers (SmA_2), while Dopa-derived ILCs with three side chains formed columnar (Col_h) mesophases. The mesophase ranges for Phe ILCs increased steadily with side chain lengths, for Tyr- and Dopa-based ILCs, however, size matching effects were observed. To clarify whether the mesomorphic behaviour has an impact on biological properties, cytotoxic and antibacterial activities of the ILCs were studied. Phe and Tyr ILCs exhibited much higher cytotoxicities (against the L-929 mouse fibroblast cell line) and/or antibacterial activities (against *Staphylococcus aureus*) than Dopa ILCs, which were mostly inactive. Furthermore, within each series the side chain length largely influenced the biological activity. Thus, the bulk mesophase behaviour appeared to correlate with biological properties, in particular the interactions with membranes, as shown by measuring the intracellular Ca^{2+}-concentration in human monocytic U937 cells after treatment with the amino acid-based ILCs.

Keywords amino acids, ionic liquid crystals, cytotoxicity, self-assembly, antibiotic activity

[a] Institut für Organische Chemie, Universität Stuttgart, Pfaffenwaldring 55, D-70569 Stuttgart, Germany. E-mail: sabine.laschat@oc.uni-stuttgart.de

[b] AG Compound Profiling and Screening, Helmholtz Zentrum für Infektionsforschung, Inhoffenstr. 7, D-38124 Braunschweig, Germany. E-mail: ursula.bilitewski@helmholtz-hzi.de

† Electronic supplementary information (ESI) available. See DOI:

Introduction

Ionic liquid crystals (ILCs) are ionic liquids, i.e. molten organic salts, which self-assemble into liquid crystalline phases. This mesophase formation is driven by nanosegregation of immiscible head groups, core units and tails as well as minimization of free volume.[1] The diverse phase behaviour of ILCs and their adjustable polarity, solubility and viscosity by tuning either cation or anion or both, low vapor pressure, high thermal stability and wide electrochemical window as well as anisotropic physical properties such as 1D ionic conductivity make them highly attractive for applications as electrolytes in Grätzel type dye-sensitized solar cells,[2] ion conductive materials for lithium ion batteries,[3] anisotropic NMR solvents for determination of residual dipolar couplings,[4] ordered reaction media,[5] and as electrochromic[6] and photoluminescent materials.[7]

The biological activities of ionic liquids (ILs) have been studied extensively[8–10] including their beneficial effects on enzymatic reactions.[11] However, the picture about the interaction of ILs with biological systems is still far from complete and moreover, characterized by studies of diverse aspects such as antimicrobial activity of imidazolium-based ILs,[10] conjugative transfer of antibiotic resistance genes via plasmids,[12] or cytotoxicity of lipid resembling ILs depending on cell membrane insertion and/or disruption.[8,13] Compounds, which interfere with bacterial membranes resulting either in direct disturbance of the ion homeostasis or increased penetration rates of co-administered antibiotics are particularly attractive. Bacterial membrane-disrupting antibiotics were reported to be effective against quiescent bacteria which are frequently not susceptible to antibiotics that inhibit bacterial intracellular targets.[14,15] Amino acid-containing ILs are promising candidates for this purpose. Investigations of ILs with amino acid-based cations and anions indicated an increased toxicity and the ability to induce apoptosis.[16] The anti-malaria activity of a betaine lipid from the fermentation broth of *Heterospora chenopodii* was rationalized by inducing plasmodial cell membrane disruption.[17]

It should be noted that Swamy and coworkers synthesized polar non-charged liquid crystalline *N*-acylglycines as neuroactive and anti-nociceptive constituents of biomembranes[18] as well as L-alanine alkyl esters which exist as unilamellar liposomes in an equimolar complex with SDS and are useful for drug delivery.[19]

In contrast, only little is known about the biological relevance of ILCs. In a seminal work Douce and coworkers prepared imidazolium salts with chain length dependent thermotropic mesomorphism which could be successfully used as vectors for siRNA transfection.[20] The alkyl chain length influenced mesophase formation and binding efficacy. For ILCs with C_{12} chains forming columnar hexagonal (Col_h) and bicontinuous cubic (Cub_{bi}) phases a better siRNA encapsulation was found than for ILCs with C_{18} chains forming only a Col_h phase. More recently, ethoxyether-functionalized imidazolium salts, especially with longer alkyl chains (C_{16} and C_{18}) forming lamellar SmA phases, were reported by Lin to exhibit anti-microbial activity against infectious bacteria.[21] While chain lengths as well as the type of supramolecular self-assembly, e.g. lamellar vs. columnar mesophase, seem to affect the behaviour of these ILCs in the cellular environment, the interplay between molecular structure, liquid crystalline self-assembly and biological properties has not been studied in detail.

We anticipated that the ability of amino acid-derived ILCs to self-assemble into anisotropically ordered supramolecular arrays such as bilayers or micellar arrangements, should have an impact on their biological properties such as interactions with membranes and other cellular structures. However, a prerequisite is a detailed understanding of the liquid crystalline self-assembly of neat amino acid-derived ILCs. Initial studies on tyrosine-derived ILCs **Tyr(m,n)** (Scheme 1) revealed some analogies to the phase behaviour of thermotropic ILCs and lyotropic liquid crystals.[22] Taking inspiration from the packing theory developed by Israelachvili[23] for hydrocarbon amphiphiles and Tschierske's work on lyotropic liquid crystals,[24] derivatives **Tyr(m,n)** (m = n) were tailored to obtain different cross sectional areas depending on the size of the counterion and thus the effective head group size. In this way

either lamellar like (SmA_2) or micellar like aggregates (Col) resulted.[22] In order to get access to further amino acid ILCs with *C*-terminal chains we aimed at guanidinium salts, which should be prepared from phenylalanine (Phe), tyrosine (Tyr) or 3,4-dihydroxyphenylalanine (DOPA). In the current study it was of interest to know whether the total number of alkoxy side chains would have an influence on the size of the cross sectional area of the alkyl tails, thus affecting the type of liquid crystalline self-assembly. Furthermore, we were interested to study whether such structural modifications have an impact on biological properties of these three series of amphiphilic compounds.

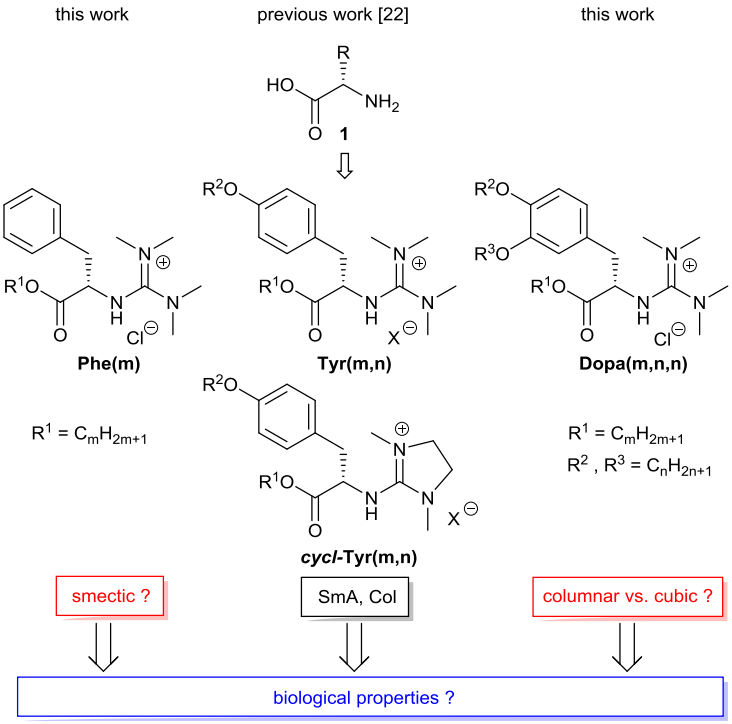

Scheme 1

Results and discussion

Synthesis of ILCs

The synthesis of the amino acid-derived ILCs is outlined in Scheme 2. Esterification of phenylalanine **1a**,[25] followed by treatment with the known tetramethylformamidinium chloride **5**[26] in the presence of $NaHCO_3$ provided the phenylalanine-based guanidinium ILCs

Phe(m). The synthesis of ILC series **Tyr(10,n)** starting from tyrosine **1b** followed the previously published procedure[22] for **Tyr(m,n)** and ***cycl*-Tyr(m,n)** with acyclic and cyclic head group, respectively. In an analogous manner Dopa **1c** was submitted to esterification followed by Boc protection to yield *N*-Boc protected Dopa esters **7** as a key intermediate. Williamson etherification of **7** with alkyl bromide, subsequent deprotection of the Boc group and reaction with formamidinium chloride **5** gave the guanidinium series **Dopa(m,n,n)**.

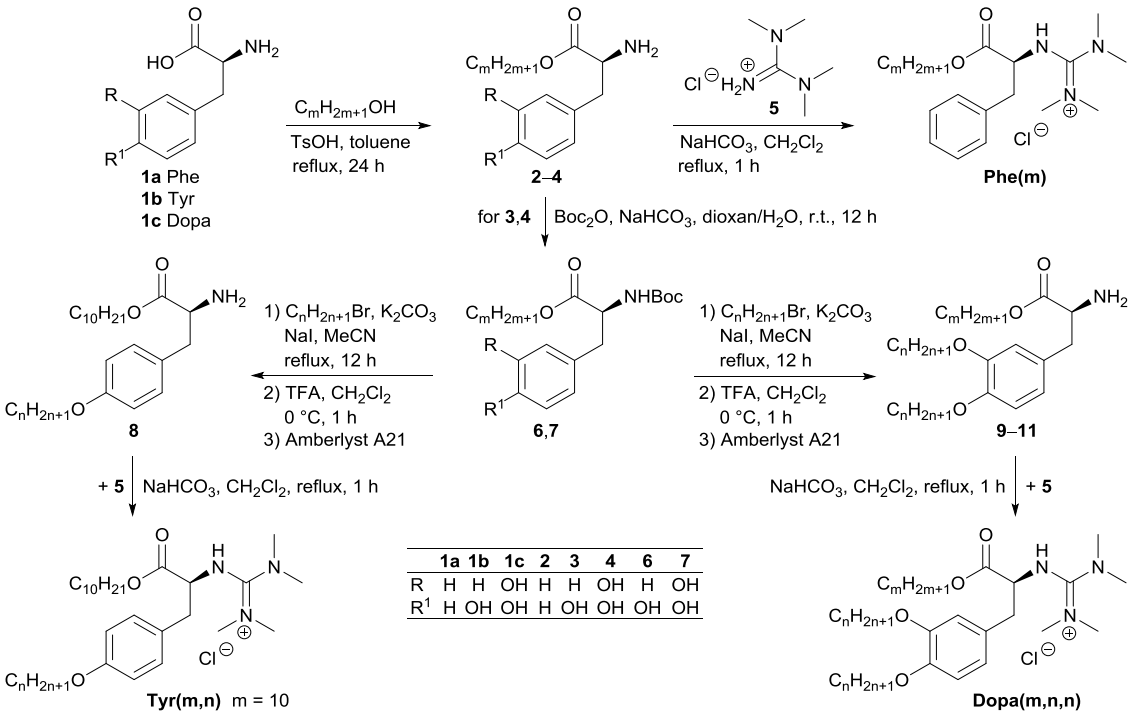

	1a	1b	1c	2	3	4	6	7
R	H	H	OH	H	H	OH	H	OH
R^1	H	OH	OH	H	OH	OH	OH	OH

Scheme 2 Synthesis of amino acid-based guanidinium ILCs **Phe(m)**, **Tyr(m,n)** and **Dopa(m,n,n)** (for details see ESI†).

Liquid crystalline self-assembly of amino acid ILCs

Mesomorphic properties of the different guanidinium salts were studied by differential scanning calorimetry (DSC), polarizing optical microscopy (POM) and X-ray diffraction (WAXS, SAXS). According to the DSC results Phe-based guanidinium chlorides **Phe(m)** with a minimum chain length of C_{12} displayed enantiotropic mesomorphism (Table 1, Fig. 1). Melting points were only little affected by the chain lengths, but the clearing points increased with increasing chain lengths from 57°C (for C_{12}) to 81°C (for C_{18}), resulting in broader mesophase widths (Fig. 1).

Table 1 Phase transition temperatures (°C) and enthalpies ΔH (kJ mol^{-1}) of phenylalanine guanidinium ILCs **Phe(m)** determined by DSC upon second cooling[a]

Entry	**Phe(m)**	Cr	T (ΔH)	SmA_2	T (ΔH)	I
(1)	**Phe(10)**	●	10	–	–	●
(2)[b]	**Phe(12)**	●	26	●	57 (0.6)	●
(3)[c]	**Phe(14)**	G	20	●	52	●
(4)	**Phe(16)**	●	26 (8.1)	●	72 (0.4)	●
(5)	**Phe(18)**	●	28 (20.0)	●	81 (0.6)	●

[a] Observed phases: glass (G), crystalline (Cr), smectic A (SmA_2), isotropic liquid (I) (heating/cooling rate 10°C min^{-1}). [b] Phase transition upon second heating. [c] In DSC curves no phase transitions visible for **Phe(14)**; transition temperatures determined by POM (cooling rate 5°C min^{-1}).

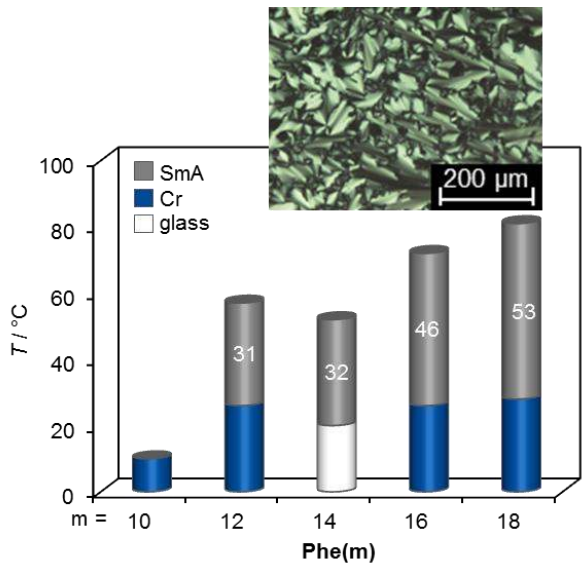

Fig. 1 Mesophase ranges of **Phe(m)** were obtained by DSC upon second cooling (m = 10, 16, 18), heating (m = 12) or by POM (m = 14) and are given in °C (cooling/heating rate 5°C min^{-1}). Inset: broken fan texture of **Phe(18)** at 97°C as seen between crossed polarizers upon cooling from the isotropic liquid (cooling rate 10°C min^{-1}, magnification ×100).

Under the POM ILCs **Phe(m)** exhibited typical broken fan textures, as exemplified for **Phe(18)** (Fig. 1). Already in the DSC studies a partial decomposition of **Phe(m)** was noticed (see ESI†). This turned out to be also the case during the long acquisition times in the SAXS experiments and thus no temperature dependent layer spacings could be obtained. However,

WAXS experiments revealed a sharp (01) reflection and a diffuse halo around 4.3 Å (Table 2, Fig. 2) indicating a SmA phase.

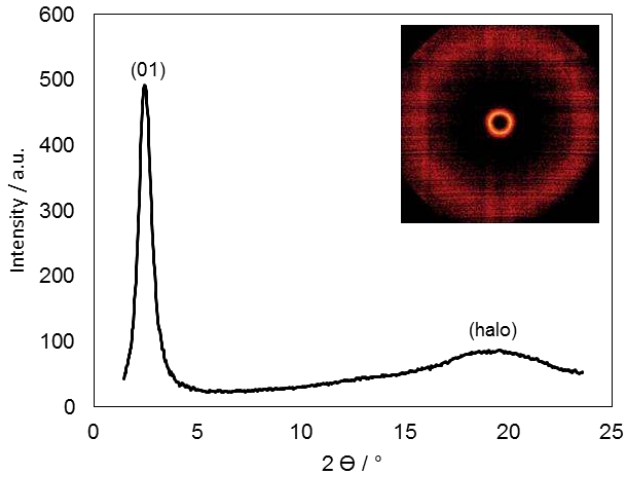

Fig. 2 X-ray scattering profile of **Phe(18)** at 80°C after cooling from the isotropic liquid (cooling rate 10°C min^{-1}). Inset: the corresponding diffraction image.

Table 2 X-ray diffraction data for Phe-based guanidinium chlorides **Phe(m)**

Entry	**Phe(m)**	Mesophase	*d* values / Å	Miller indices
(1)	**Phe(12)**	SmA_2	30.0	(01)
		at 49°C	4.3	(halo)
(2)	**Phe(16)**	SmA_2	35.6	(01)
		at 52°C	4.5	(halo)
(3)	**Phe(18)**	SmA_2	35.7	(01)
		at 69°C	4.6	(halo)

The synthesized chlorides **Tyr(10,n)** were also mesomorphic and exhibited under the POM maltese cross textures comparable to those of **Tyr(14,n)** indicating SmA mesophases as well (see ESI†).

All Dopa-based guanidinium chlorides **Dopa(m,n,n)** displayed enantiotropic mesomorphism (Table 3, Fig. S3). The phase behaviour of **Dopa(m,n,n)** was strongly controlled by the ester unit. Clearing points of the C_{10} esters **Dopa(10,n,n)** decreased from n = 6 to n = 10, then reaching a plateau value with increasing chain lengths n of the ether units (Table 3, entries 1–4). As melting points increased concurrently, the temperature range of the mesophases is reduced from 77°C (n = 6) to 5°C (n = 18). Presumably, size matching for C_{10} ester is best for

short C_6 ethers. In contrast, for C_{14} esters **Dopa(14,n,n)** (entries 5–9) the size matching effect resulted in significantly higher clearing points and mesophase widths of 58–73°C for derivatives with C_{12}–C_{18} ethers. For the series **Dopa(18,n,n)** with the longest C_{18} ester clearing points remained nearly constant upon increasing the alkoxy chain length n (entries 10–14), resulting in an overall decrease of mesophase widths from 74°C (n = 10) to 45°C (n = 18).

Comparison of **Dopa(14,n,n)** with the known tyrosine C_{14} ester **Tyr(14,n)**[22] reveals that the size matching also affected mesophase ranges in this tyrosine series, but the tyrosine C_{14} ester tolerated a broader variation of ether chain lengths while keeping melting and clearing points relatively constant.[22]

Table 3 Phase transition temperatures (°C) and enthalpies ΔH (kJ mol^{-1}) of Dopa ILCs **Dopa(m,n,n)** as determined by DSC upon second cooling[a]

Entry	**Dopa(m,n,n)**	Cr	T (ΔH)	Col_h	T (ΔH)	I
(1)[b]	**Dopa(10,6,6)**	●	18	●	95	●
(2)	**Dopa(10,10,10)**	●	21 (1.2)	●	46 (0.8)	●
(3)	**Dopa(10,14,14)**	●	29 (9.3)	●	46 (0.8)	●
(4)	**Dopa(10,18,18)**	●	45 (42.6)	●	50 (0.6)	●
(5)	**Dopa(14,10,10)**	●	28 (1.9)	●	54 (1.1)	●
(6)	**Dopa(14,12,12)**	●	52 (46.7)	●	119 (1.5)	●
(7)	**Dopa(14,14,14)**	●	61 (52.6)	●	134 (1.6)	●
(8)	**Dopa(14,16,16)**	●	60 (52.3)	●	118 (1.0)	●
(9)	**Dopa(14,18,18)**	●	59 (60.8)	●	126 (1.6)	●
(10)	**Dopa(18,10,10)**	●	38 (25.2)	●	112 (1.0)	●
(11)	**Dopa(18,12,12)**	●	35 (19.4)	●	113 (2.3)	●
(12)[b]	**Dopa(18,14,14)**	●	50	●	110	●
(13)	**Dopa(18,16,16)**	●	70 (62.2)	●	112 (1.2)	●
(14)	**Dopa(18,18,18)**	●	75 (81.5)	●	120 (1.2)	●

[a] Observed phases: crystalline (Cr), hexagonal columnar (Col_h), isotropic liquid (I) (heating/cooling rate 10°C min^{-1}). [b] No phase transitions visible in the DSC of **Dopa(10,6,6)** and **Dopa(18,14,14)**; transition temperatures were determined by POM (cooling rate 5°C min^{-1}).

Under the POM fan-shaped textures, e.g. **Dopa(10,10,10)**, focal conic textures, e.g. **Dopa(14,18,18)** and broken focal conic textures, e.g. **Dopa(18,18,18)** or **Dopa(18,10,10)** (Fig. 3a–d) were observed, which are typical for columnar mesophases.

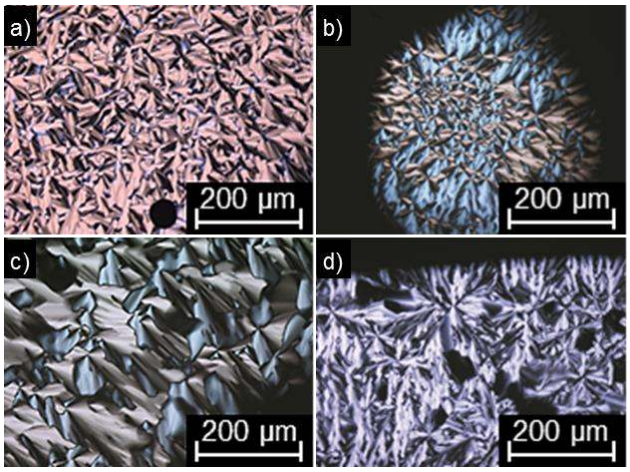

Fig. 3 POM images of Dopa ILCs as seen between crossed polarizers upon cooling from the isotropic liquid (cooling rate 10°C min^{-1}, magnification ×100). a) **Dopa(10,10,10)** at 85°C, b) **Dopa(14,18,18)** at 100°C, c) **Dopa(18,18,18)** at 108°C and d) **Dopa(18,10,10)** at 110°C.

XRD studies revealed Col_h phases for all guanidinium ILCs **Dopa(m,n,n)** (Table 4). An illustrative example are the 2D diffraction profile and XRD pattern of **Dopa(14,14,14)** (Fig. 4).

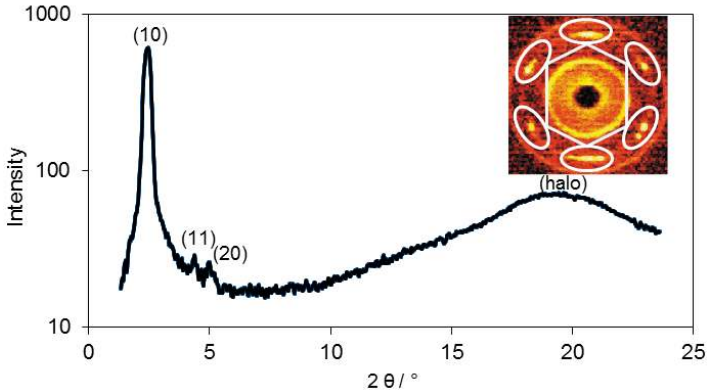

Fig. 4 2D X-ray diffraction profile of Dopa ILC **Dopa(14,14,14)** at 85°C upon cooling from the isotropic phase (cooling rate 10°C min^{-1}). Inset: the corresponding diffractogram.

In the small-angle region three distinct reflections in a ratio of 1 : 1/√3 : 1/√4 are visible, which were indexed as (10), (11) and (20) characteristic of a hexagonal columnar mesophase. In the wide-angle region a broad halo around 4.6 Å was detected, which was rotated by 90°

and corresponds to the disordered alkyl chains. In the diffractogram (Fig. 4, inset) a hexagon is visible indicating the presence of an ordered sample. Surprisingly, the hexagon pattern was found in the (11) reflex rather than the (10) reflex. Presumably, this diffractogram is caused by a superposition of ordered and non-ordered reflections.

Table 4 X-ray diffraction data of Dopa ILCs **Dopa(m,n,n)**

Entry	**Dopa(m,n,n)**	Phase	Lattice parameter / Å	Layer spacing / Å[a]	Miller indices	*Z*
(1)	**Dopa(10,10,10)**	Col_h	a = 41.0	35.7	(10)	5
		p6mm	at 40°C	20.5 (20.6)	(11)	
				18.0 (17.9)	(20)	
				4.4	(halo)	
(2)	**Dopa(10,14,14)**	Col_h	a = 45.8	39.6	(10)	6
		p6mm	at 45°C	22.6 (22.9)	(11)	
				19.6 (19.8)	(20)	
				4.6	(halo)	
(3)	**Dopa(10,18,18)**	Col_h	a = 49.3	42.7	(10)	6
		p6mm	at 55°C	24.5 (24.7)	(11)	
				21.2 (21.4)	(20)	
				4.5	(halo)	
(4)	**Dopa(14,10,10)**	Col_h	a = 39.5	34.2	(10)	5
		p6mm	at 64°C	19.5 (19.7)	(11)	
				16.8 (17.1)	(20)	
				4.6	(halo)	
(5)	**Dopa(14,14,14)**	Col_h	a = 41.7	36.2	(10)	5
		p6mm	at 85°C	20.2 (20.8)	(11)	
				17.6 (18.0)	(20)	
				4.6	(halo)	
(6)	**Dopa(14,16,16)**	Col_h	a = 43.0	37.3	(10)	5
		p6mm	at 88°C	21.5 (21.5)	(11)	
				18.6 (18.6)	(20)	
				4.6	(halo)	
(7)	**Dopa(14,18,18)**	Col_h	a = 42.3	36.6	(10)	5
		p6mm	at 85°C	21.2 (21.1)	(11)	
				18.1 (18.3)	(20)	
				4.6	(halo)	
(8)	**Dopa(18,10,10)**	Col_h	a = 42.6	36.9	(10)	5
		p6mm	at 65°C	20.4 (20.2)	(11)	
				17.8 (17.5)	(20)	
				4.6	(halo)	
(9)	**Dopa(18,12,12)**	Col_h	a = 36.3	31.4	(10)	4
		p6mm	at 85°C	18.1 (18.1)	(11)	
				4.6	(halo)	

(10)	**Dopa(18,14,14)**	Col_h	a = 45.0	39.0	(10)	5
		p6mm	at 73°C	22.5 (22.5)	(11)	
				19.4 (19.5)	(20)	
				4.6	(halo)	
(11)	**Dopa(18,16,16)**	Col_h	a = 45.7	39.6	(10)	5
		p6mm	at 76°C	22.8 (22.8)	(11)	
				19.8 (19.8)	(20)	
				4.6	(halo)	
(12)	**Dopa(18,18,18)**	Col_h	a = 46.3	40.1	(10)	5
		p6mm	at 70°C	23.0 (23.1)	(11)	
				20.0 (20.0)	(20)	
				4.6	(halo)	

[a] Calculated values in parentheses.

Comparison of the two series **Phe(m)**, **Dopa(m,n,n)** with the previously reported **Tyr(m,n)** chlorides[22] revealed that the number of side chains determined the mesophase type (Fig. 5).

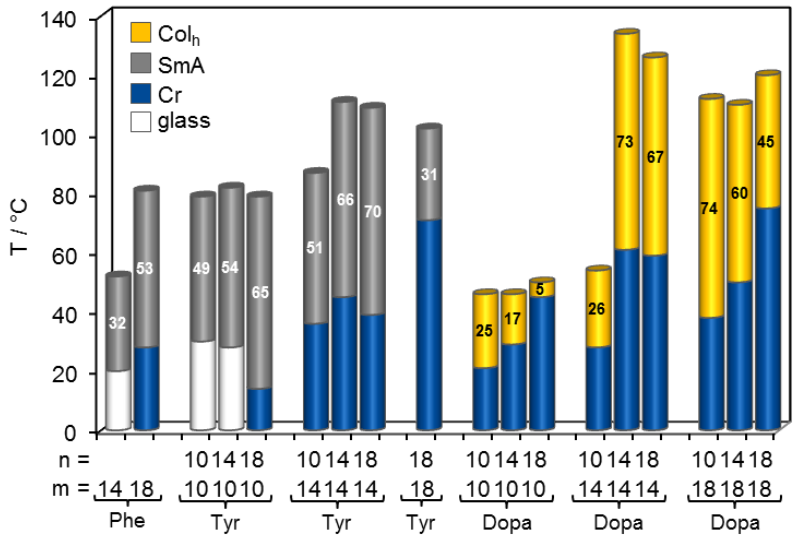

Fig. 5 Comparison of mesophase type and mesophase range (given in °C) for selected examples from the series **Phe(m)**, **Tyr(m,n)**, and **Dopa(m,n,n)**. The values for **Tyr(10,10)**, **Tyr(14,n)** and **Tyr(18,18)** are taken from ref.[22]

Phenylalanine- and tyrosine-based guanidinium ILCs **Phe(m)** and **Tyr(m,n)** with one or two side chains favor lamellar self-assembly (SmA), while Dopa-based ILCs **Dopa(m,n,n)** exclusively self-assemble into columnar mesophases (Col_h). Despite their increased interfacial curvature caused by the presence of three side chains no evidence for cubic phases was found in

contrast to previous reports on wegde-shaped ILCs by Cheng, Tschierske and Percec, respectively.[27,28] In addition the number of side chains contributes to the mesophase stability, as evidenced from the clearing points increasing within the series **Phe(m)<Tyr(m,n)<Dopa(m,n,n)** except for Dopa ILCs with C_{10} ester. However, the phase range is strongly affected by the chain lengths of ester and ether unit.

In order to rationalize the XRD results, molecular lengths of the members of the different series were calculated by using the AVOGADRO program.[29] Taking into account the above mentioned difficulties for the phenylalanine ILCs caused by thermal decomposition smectic layer distances increased with increasing chain lengths from 30 Å for **Phe(12)** to 35.6 Å and 35.7 Å for **Phe(16)** and **Phe(18)** (Table 2) in agreement with a SmA_2 bilayer model analogously to tyrosine derivatives **Tyr(m,n)** with chloride counterion[22] (Fig. 6a).

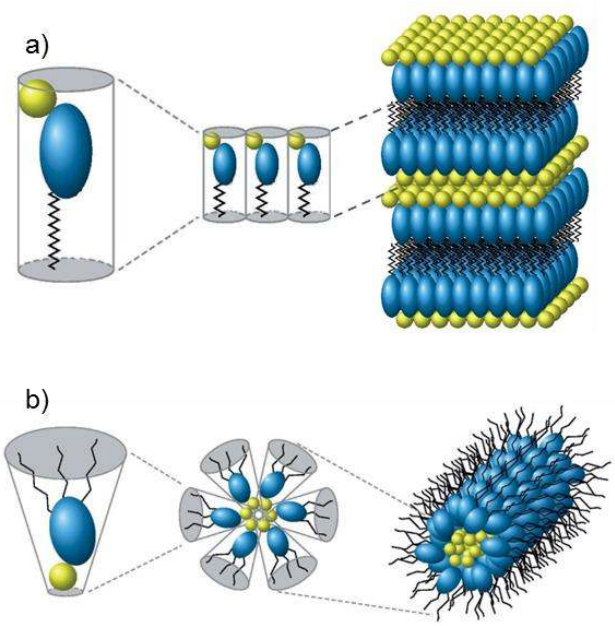

Fig. 6 Schematic representation of the proposed packing models of a) phenylalanine ILCs **Phe(m)** and b) Dopa ILCs **Dopa(m,n,n)** considering Israelachvili's methodology.[23] Cationic core with guanidinium head group (blue), counterion chloride (yellow).

In a similar fashion the effective volume of the head group and the molecular lengths of the Dopa ILCs **Dopa(m,n,n)** were calculated in comparison with tyrosine esters **Tyr(m,n)**[22] considering the packing model by Israelachvili.[23] The presence of three alkyl side chains in

Dopa(m,n,n) resulted in a cone-shape of the mesogen, leading to inversed micellar-type self-organized discs, where each disc is composed of 5 or 6 mesogens (Figure 6b). The absence of any cubic phases in ILCs **Dopa(m,n,n)** might be rationalized in a similar way as was proposed previously by Kato for L-glutamate-derived imidazolium ILCs[30] and Ohno for lyotropic amino acid ionic liquid/amphiphile mixtures,[31] that intermolecular hydrogen bonds are required for the formation of curved ionophilic/ionophobic interfaces present in bicontinuous cubic mesophases. Thus, in the case of **Dopa(m,n,n)**, the interfacial curvature required for formation of columnar phases is solely due to the cone shape of the molecules caused by the steric bulkiness of the three alkyl side chains.

Biological properties of amino acid ILCs

In order to evaluate the biological properties of the amino acid-derived guanidinium ILCs **Phe(m)**, **Tyr(m,n)**, and **Dopa(m,n,n)**, their cytotoxic activity was probed first. Inhibition of proliferation of the L-929 mouse fibroblast cell line was investigated by the WST-1 cytotoxicity assay (ESI†).[32]

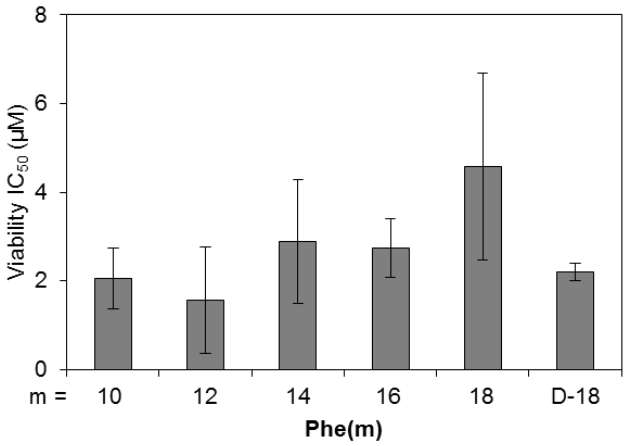

Fig. 7 Dependence of the antiproliferative activity of phenylalanine-based ILCs **Phe(m)** (IC_{50} values) on the length of the alkoxy chain. For comparison the non-mesomorphic derivative **Phe(10)** is included.

Among the phenylalanine ILCs **Phe(m)** all members of the series were active with IC_{50} values in the range of 1–5 μM independent of the mesomorphic structure. For a selected ILC

Phe(18) the influence of the amino acid configuration on the biological activity was investigated. Remarkably, derivatives L-**Phe(18)** and D-**Phe(18)** with unnatural D-configuration yielded similar IC_{50} values (Fig. 7). The similar cytotoxicity might be caused by the amphiphilic character of the phenylalanine-derived ILCs rather than specific formation of diastereomeric ILC-protein aggregates. However, due to the fact that only one pair of enantiomeric ILCs was tested, it is too early to draw further conclusions.

The cytotoxic activity of tyrosine guanidinium chlorides **Tyr(m,n)** showed a pronounced influence of the chain lengths m and n. The symmetrical ILCs **Tyr(10,10)** and **Tyr(14,14)** (m = n) were rather active against the mouse fibroblast cell line L-929 yielding IC_{50} values of 2.8 μM and 9.1 μM, respectively (Fig. 8). A similar result was obtained for both analogues with cyclic head group ***cycl*-Tyr(10,10)** and ***cycl*-Tyr(14,14)** (IC_{50} = 3.7 μM) (ESI†).

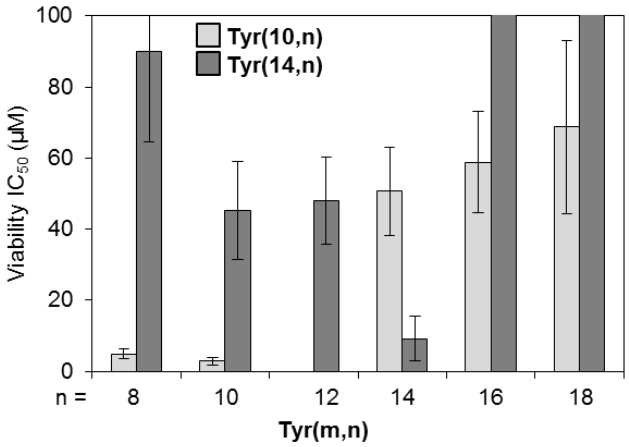

Fig. 8 Dependence of the antiproliferative activity of tyrosine-based ILCs **Tyr(10,n)** and **Tyr(14,n)**[22] on the length of the ether chain.

In the case of unsymmetrical ILCs, only **Tyr(10,8)** with a minor difference between the lengths of the two chains was tolerated for good activity (IC_{50} 4.9 μM), whereas the other members were almost inactive (IC_{50} ≥45 μM) (Fig. 8). Thus, tyrosine-based ILCs **Tyr(m,n)** showed no significant cytotoxicity, when the chain lengths exceeded 14 CH_2 groups and when the difference in chain lengths between ether and ester chain was more than 2 CH_2 groups. This is in good agreement with previous studies, which showed that the cytotoxicity of ionic

liquids increased with increasing chain lengths up to a threshold and then decreased again upon further chain elongation.[8] For example, 1-alkylquinolinium bromides with a minimum chain length of C_8 displayed cytotoxic effects on murine fibroblast cells and C_{14} derivatives showed the highest activity which somehow leveled out or even decreased upon further elongating the side chain.[33]

Within the ILCs **Dopa(m,n,n)** with equal chain lengths (m = n) only **Dopa(18,18,18)** showed some activity (IC_{50} 22 μM) (Fig. 9). In contrast **Dopa(10,10,10)** and **Dopa(14,14,14)** were inactive.

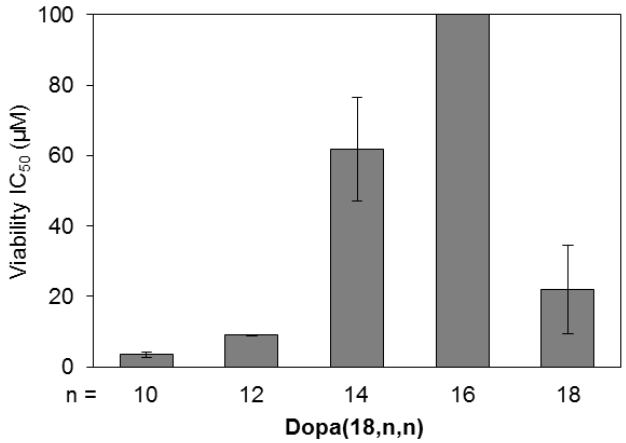

Fig. 9 Dependence of the antiproliferative activity of the **Dopa(18,n,n)** derived ILCs on the lengths of the ether chain.

This was also true for **Dopa(m,n,n)** derivatives with unequal chain lengths ($m \neq n$). Here, the chain lengths of the ester moiety seem to be particularly critical, as derivatives with 10 or 14 CH_2 groups were largely inactive, whereas an unsymmetrical substitution pattern was tolerated for derivatives **Dopa(18,n,n)** (Fig. 9). Illustrative examples are **Dopa(18,10,10)** (IC_{50} 3.5 μM) vs. **Dopa(10,18,18)** (IC_{50} 14.9 μM) vs. **Dopa(14,18,18)** (IC_{50} >100 μM).

Antibacterial activities of amino acid ILCs were determined by broth microdilution assays measuring the inhibitory effect on the growth of Gram-positive methicillin-sensitive *Staphylococcus aureus*, and Gram-negative *Escherichia coli* K12. None of the compounds showed significant activity on *E. coli* K12 (data not shown). In general, phenylalanine ILCs

Phe(m) displayed higher antibiotic activity on *S. aureus* than tyrosine (**Tyr(m,n)**) and Dopa ILCs **Dopa(m,n,n)**, respectively. The IC_{50} values of ILCs **Phe(m)** ranged between 4 and 15 μM (Fig. 10a). However, in comparison to their cytotoxicities, the length of the ester chain influenced the antibacterial activity: The most active ILCs were **Phe(12)** and **Phe(14)** with IC_{50} values of 8 μM and 4 μM, respectively. Increasing the chain lengths led to slightly reduced activities (Figure 10a). It should be emphasized that **Phe(10)** with the shortest chain length, which is devoid of any mesomorphism, was the least active member (IC_{50} = 21 μM). Our results are in good agreement with previous work by Musumarra who studied the chain lengths dependence of alkylimidazolium ionic liquids regarding biological activity. Derivatives with medium chain lengths were reported to serve as threshold and provided the highest antimicrobial activity, while the activity decreased upon further chain elongation.[34]

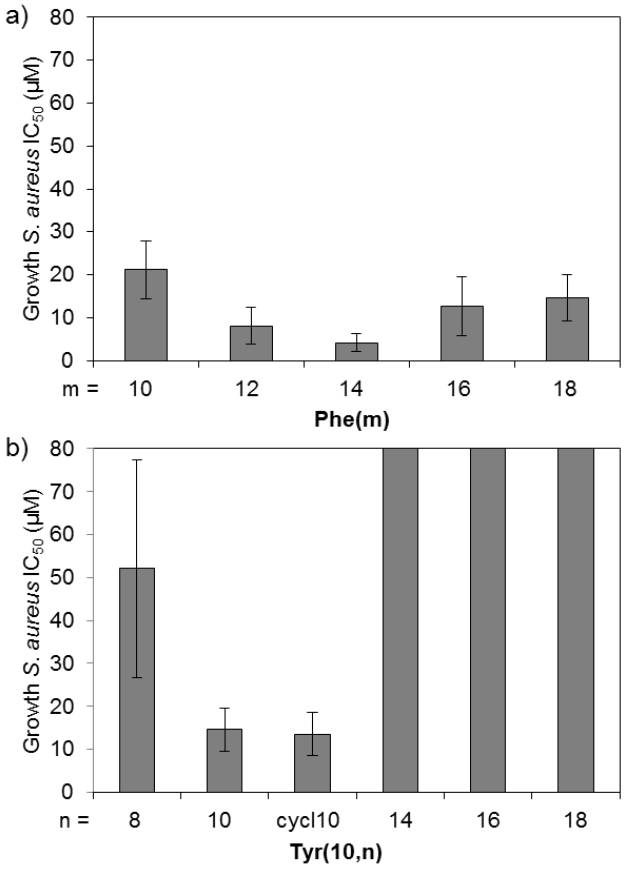

Fig. 10 Antibacterial activity of amino acid guanidinium chlorides **Phe(m)** (a) and **Tyr(10,n)** (b) against *S. aureus* determined by broth microdilution assay (ESI†). The non-mesomorphic **Phe(10)** was included for comparison.

In the case of the tyrosine ILCs **Tyr(m,n)**, only medium antibiotic activity against *S. aureus* was observed, that was limited to the symmetrical short chain derivatives **Tyr(10,10)** and ***cycl*-Tyr(10,10)** (IC_{50} = 13–14 μM) (Fig. 10b). A comparison of the series **Phe(m)** and **Tyr(10,n)** demonstrates that IC_{50} values follow a "minimum curve", i.e. for certain chain lengths the highest activity was found. All other ILCs including **Tyr(14,n)** and the Dopa series **Dopa(m,n,n)** were inactive.

Due to their structural similarity with natural occurring lipids such as 1,2-dipalmitoyl-sn-glycerol-3-phosphocholine or surfactants such as *N*-[1-(2,3-dioleyloxy)propyl]-*N,N,N*-tri-methylammonium chloride and recently reported imidazolium salts[13] the maintenance of the membrane integrity of mammalian cells was evaluated after treatment of the cells with single concentrations of selected ILCs. Intact membranes of mammalian cells do not allow the passage of cations by diffusion, but only by ion channel or ion transport proteins or by iono-phors. Thus, concentration gradients can be maintained between the intracellular and the extracellular space. Particularly, intracellular concentrations of free Ca^{2+}-ions are low (in the nM range) so that a steep Ca^{2+}-ion concentration gradient is established, when cells are maintained in a Ca^{2+}-containing buffer or medium, and Ca^{2+}-ion concentrations rapidly increase, when the cell membrane becomes leaky or when the compound has Ca^{2+}-ionophor activities. Intracellular Ca^{2+}-concentrations can be detected using the Ca^{2+}-indicator dye Fluo-4[35] in the Fluo-4 NW assay. We loaded the human monocytic cell line U937 with the dye according to the manufacturer's instructions and monitored the increase in fluorescence after incubation with the respective ILC. The ILCs **Phe(12)**, **Phe(16)**, D-**Phe(18)**, **Tyr(10,n)**, **Tyr(14,12)**, and **Dopa(14,10,10)** indeed led to Ca^{2+}-influx indicating interactions with the cell membrane (Fig. 11). However, if membrane damage were the only mode of action of the ILCs, low IC_{50} values should correlate with high fluorescence values due to Ca^{2+}-influx. This is not given for all compounds. Moreover, it has to be considered that the chosen concentrations were usually in the range of 80–120 μM, i.e. higher than the IC_{50} values so that

secondary effects cannot totally be excluded. On the other hand, incubation times between compounds and cells were only 3 h, whereas cytotoxicity data were based on incubation times of 3 days.

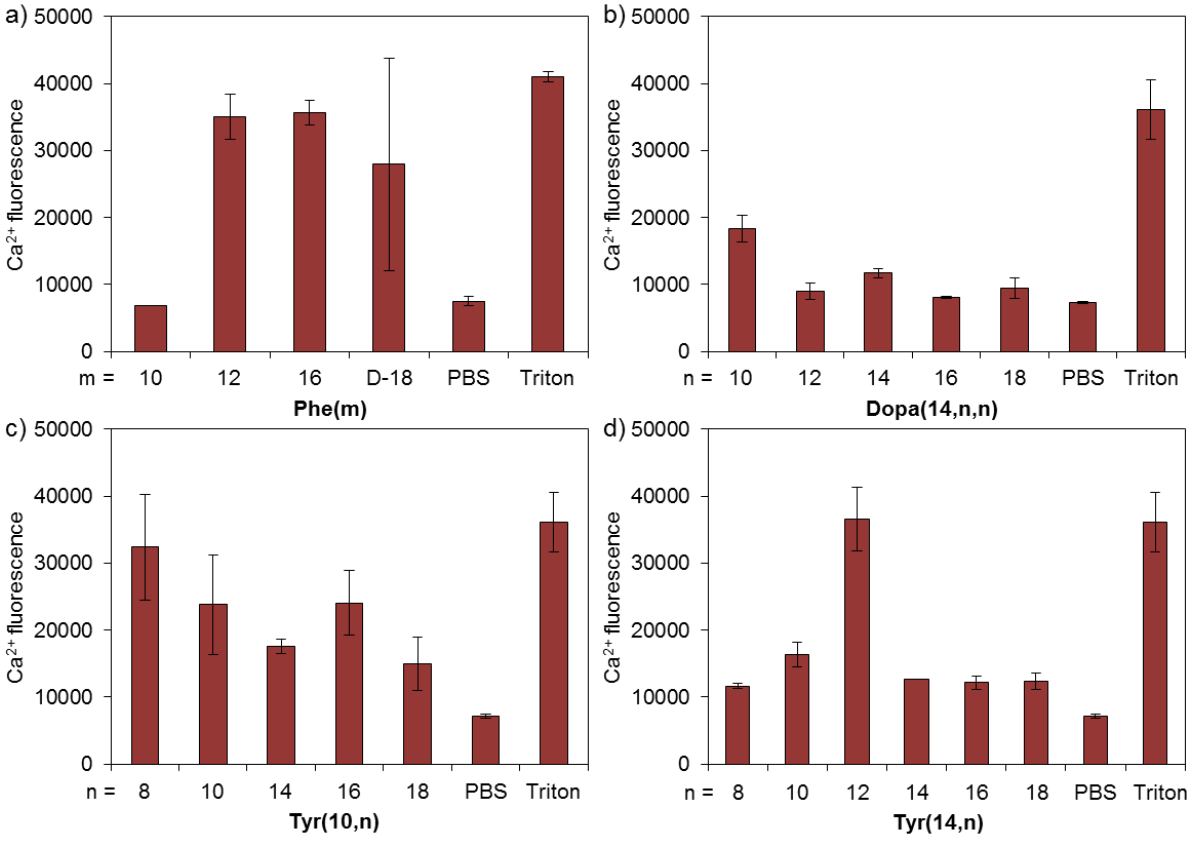

Fig. 11 Intracellular Ca^{2+}-concentrations in U937 cells resulting from cellular treatment with various ILCs for 3 h. Cells were loaded with the Ca^{2+}-specific dye Fluo-4 prior to ILC treatment, fluorescence ($\lambda_{max,exc}$ = 485 nm; $\lambda_{max,em}$ = 528 nm) was determined with a fluorescence microtiter plate reader (Synergy4, Biotek) (ESI†) and was taken as measure of Ca^{2+}-concentrations. The values resulting from treatment with phosphate buffered saline (PBS) (0%) and triton (100%) are given as reference. **Dopa(m,n,n)** series (m = 10, 18) did not show increased Ca^{2+}-concentrations.

For selected ILCs **Phe(m)** and **Tyr(10,10)** membrane permeability was also assessed by employing the propidium iodide (PI) assay according to Vylkova.[36] Due to its dicationic structure PI can only pass through defect membranes and then intercalate with cellular DNA allowing differentiation of free and intercalated dye through their different absorption and emission characteristics. Partial staining with PI of ILC-treated L-929 cells populations was

observed. After treatment with **Phe(m)** 30% (m = 12), 60% (m = 14), 48% (m = 16) and 25% (m = 18) of the cell population was stained and 52% after treatment with **Tyr(10,10)**. Cytotoxicity of these particular derivatives was also studied by the Lactate dehydrogenase (LDH) assay.[37] The presence of LDH in cell supernatants is an indicator of cytotoxicity, as this enzyme usually is absent from cell culture media and is released only from damaged cells. In agreement with the PI test, ILCs **Phe(12)**, **Phe(14)**, **Phe(16)** and **Tyr(10,10)** showed a positive response in the LDH assay.

According to a report by Chung micelle-formation of pharmaceutical compounds can interfere with their biological activity, sometimes camouflaging their inherent mode of action.[38] Following his protocol for suppression of micellar aggregates, we performed the proliferation tests for selected ILCs **Phe(12)**, **Phe(16)**, **Tyr(10,10)** and **Dopa(18,10,10)** in the presence of the commercially available detergents CHAPS and Tween, respectively. In the case of **Phe(12)** and **Phe(16)**, IC_{50} values remained relatively constant (1.1 μM and 5 μM) as compared to the incubation experiments without detergent (approximately 2 μM and 3 μM, Fig. 7), whereas the cytotoxicity of **Tyr(10,10)** and **Dopa(18,10,10)** disappeared upon addition of the detergents (IC_{50} > 100 μM) vs. detergent-free experiments (IC_{50} = 2.8 μM and 3.5 μM, Figs. 8, 9). These results suggest that the observed cytotoxicity of **Tyr(10,10)** and **Dopa(18,10,10)** is mainly caused by micellar aggregates in contrast to **Phe(12)**, **Phe(16)**, where micelle formation does not seem to play a role.

In order to gain some preliminary information on the aggregation behaviour of amino acid-derived ILCs in solution, circular dichroism (CD) spectra of selected ILCs were recorded (Fig. 12). Comparison of the CD spectra of ILC **Phe(14)** with its free amino acid L-Phe revealed a bathochromic shift of the positive CD signal (Fig. 12a). In the case of tyrosine-based ILCs **Tyr(12,12)**, **Tyr(14,14)**, **Tyr(18,18)**,[22] also bathochromic shifts were observed with respect to the parent L-Tyr (Fig. 12b). Furthermore, CD spectra were only little affected by

the chain lengths. A similar outcome was obtained for ILCs **Dopa(m,10,10)** (m = 10, 14, 18) with respect to the free amino acid L-Dopa (Fig. 12c).

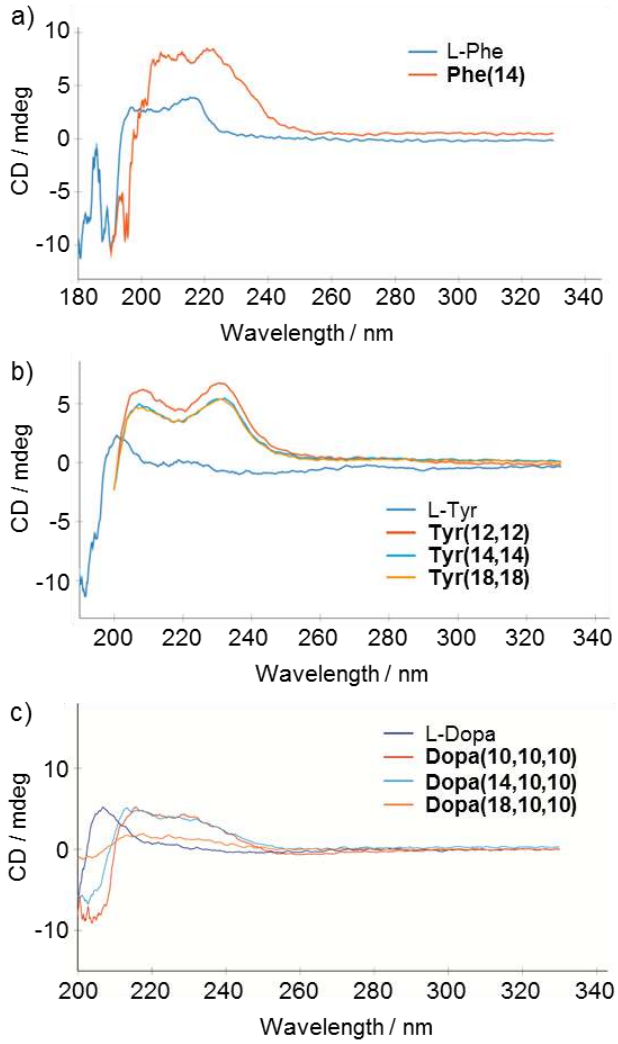

Fig. 12 CD spectra of selected ILCs **Phe(14)**, symmetrical **Tyr(m,n)** (m = n = 12, 14,18),[22] **Dopa(m,10,10)** (m = 10, 14, 18) (CH_3CN, c = 4 μmol L^{-1}) and their corresponding free amino acids L-Phe, L-Tyr and L-Dopa (H_2O, c = 0.4 μmol/L).

Taking into consideration the recent CD studies on amino acids by Amdursky and Stevens,[39] the observed bathochromic shift of the amino acid-derived ILCs **Phe(m)**, **Tyr(m,n)** and **Dopa(m,n,n)** with respect to their neat amino acids might be caused by the guanidinium head group. Electrostatic interactions of the head groups and chloride counterions together with intermolecular hydrogen bonds between the guanidinium N–H and Cl^- as well as π–π-interactions of the electron-rich aromatic units might lead to aggregation not only in CH_3CN

solution but also in an aqueous medium. However, further detailed studies are required to investigate such aggregation behaviour under aqueous conditions.

Conclusion

We provided a convenient synthetic access to a series of amino acid-derived ILCs **Phe(m)**, **Tyr(10,n)** and **Dopa(m,n,n)**, whose mesomorphic properties were investigated. From comparison with tyrosine-derived ILCs **Tyr(m,n)** and ***cycl*-Tyr(10,10)**[22] it is obvious that the mesophase type was determined by the total number of side chains attached to the amino acid core. Phenylalanine ILCs **Phe(m)** with a single alkoxy chain at the ester moiety as well as tyrosine chlorides **Tyr(m,n)** with two alkoxy chains at the ester and ether moiety self-assembled into bilayer SmA_2 phases. In the case of the Dopa ILCs **Dopa(m,n,n)** with three alkoxy chains, the increased volume requirements of the hydrophobic segment of these ILCs resulted in an inverse micellar-like self-assembled structure forming a Col_h phase and the mesophase ranges were governed by the lengths of the side chains.

In contrast to the experimental structure–property relationships regarding the mesomorphic properties, the correlation of the molecular structure and/or liquid crystalline self-assembly of the amino acid-derived ILCs with their biological properties is less clear cut. Cytotoxicity studies revealed an efficient ability of all phenylalanine ILCs **Phe(m)** to inhibit the proliferation of the L-929 mouse fibroblast cell line. However, for the **Tyr(10,n)** series with a C_{10} ester chain short ether chain lengths (C_8, C_{10}) were beneficial. In contrast, medium ether chain lengths (C_{12}, C_{14}) were beneficial for the **Tyr(14,n)** series with a C_{14} ester chain, suggesting that there is a size matching effect in a similar fashion as was observed for the mesomorphic properties.[22] A similar tendency was found for the Dopa series **Dopa(m,n,n)**, differing in the ester chain length (m = 10, 14, 18). It should be emphasized that selected ILCs **Phe(12)** and **Phe(16)** retained their cytotoxic activities even in the presence of detergents CHAPS and Tween. Therefore, micelle formation of the ILC is probably not involved in the

cytotoxic activity. An alternative explanation might be that the interaction between the guanidinium ILCs and the membrane lipids is rather strong and not even disturbed by the presence of detergents. The evaluated ILCs **Tyr(10,10)** and **Dopa(18,10,10)**, however, completely lost their activities upon addition of the detergents, suggesting that the observed low cytotoxicity of some tyrosine and Dopa derivatives is mainly due to micellar self-assembly. The observation that the Dopa ILCs were less active than Phe- and Tyr-derived ones might be explained by recent studies by Litwinienko on dopamine, which presumably does not penetrate the bilayer membrane, but interacts superficially with the biomembrane.[40]

Within the phenylalanine series ILCs **Phe(12)**, **Phe(14)** effectively inhibited the growth of *Staphylococcus aureus*, whereas shorter ether chains (C_8, C_{10}) were required for the anti-biotic activity of tyrosine derivatives **Tyr(10,n)**. All other amino acid ILCs were inactive, suggesting that there is again a size matching effect operative.

Based on previous reports by Bazan,[41] that pendant ionic groups of conjugated oligo-electrolytes enable the intercalation into membranes and studies by Futaki,[42] that amphiphilic counterions such as pyrene butyrate actively induce membrane curvature and perturb lipid packing of biological membranes, we anticipated that the observed biological acitivities of the amino acid-derived ILCs might be due to their interaction with membranes. Indeed, Ca^{2+}-influx was observed after treatment of cells with several ILCs indicating the formation of pores in the cell membrane. These results were supported by PI and LDH detection after cell treatment with selected ILCs.

As recently discussed by Walkenhorst[43] and Epand[44] the bacterial membrane provides a promising target for novel antimicrobials. However, different molecular mechanisms have to be considered, such as inhibition of lipopolysaccharides or altering membrane permeability, morphology or curvature. Previous SAR studies on cationic diamines by Woster revealed that electrostatic interactions of these diamines with the negatively charged bacterial membrane increased the permeability and led to depolarisation, resulting in bacterial cell lysis.[45] Our

work suggested that ILCs with cationic head groups might be developed to bioactive compounds with specific activities. In particular the interaction of the compounds with the membranes of different organisms (e.g. mammalian cells and bacteria) has to be investigated in more detail, tailoring cationic head groups, core units, side chains and counterions to improve the selectivity of the activity. Starting points could be, for example, the observations that **Phe(12)** displays both cytotoxic activity, membrane permeabilization and pronounced antimicrobial activity. Thus, future work is necessary to elucidate the biological mode of action of amino acid-derived ILCs.

Acknowledgement

Generous financial support by the Deutsche Forschungsgemeinschaft (LA 907/17-1), the Ministerium für Wissenschaft, Forschung und Kunst des Landes Baden-Württemberg, the Bundesministerium für Bildung und Forschung (shared instrumentation grant 01 RI05177), the Carl-Schneider-Stiftung Aalen, the Alfred Kärcher Förderstiftung and the Fonds der Chemischen Industrie are gratefully acknowledged. The biological assays significantly benefitted from the excellent technical assistance of Brigitte Pawletta (COPS, HZI). We would like to thank Prof. Frank Giesselmann for valuable discussions.

Conflicts of interest

There are no conflicts to declare.

References

1 Reviews: (*a*) K. Goossens, K. Lava, C. W. Bielawski and K. Binnemans, *Chem. Rev.*, 2016, **116**, 4643–4807; (*b*) M. Mansueto, S. Laschat, in *Handbook of Liquid Crystals*, 2nd ed., ed. J. W. Goodby, P. J. Collings, T. Kato, C. Tschierske, H. Gleeson and P. Raynes, Wiley-VCH, Weinheim, 2014, Vol. 6, pp 231–280; (*c*) S. K. Pal and S. Kumar, in *Biosensors Nanotechnology*, ed. A. Tiwari and A. P. F. Turner, Scrivener Publishing, Beverly/MA, 2014, pp 267–314; (*d*) S. Chen and S. H. Eichhorn, *Isr. J. Chem.*, 2012, **52**,

830–843; (*e*) V. Causin and G. Saielli, in *Green Solvents II: Properties and Applications of Ionic Liquids*, ed. A. M. Inamuddin, Springer, Dordrecht, 2012, pp 79–118; (*f*) K. V. Axenov and S. Laschat, *Materials*, 2011, **4**, 206–259; (*g*) L. Douce, J.-M. Suisse, D. Guillon and A. Taubert, *Liq. Cryst.*, 2011, **38**, 1653–1661; (*h*) K. Binnemans, *Chem. Rev.*, 2005, **105**, 4148–4204.

2 N. Yamanaka, R. Kawano, W. Kubo, T. Kitamura, Y. Wada, M. Watanabe and S. Yanagida, *Chem. Commun.*, 2005, 740–742.

3 H. Shimura, M. Yoshio, A. Hamasaki, T. Mukai, H. Ohno and T. Kato, *Adv. Mater.*, 2009, **21**, 1591–1594.

4 (*a*) G. A. N. Gowda, H. Chen, C. L. Khetrapal and R. G. Weiss, *Chem. Mater.*, 2004, **16**, 2101–2106; (*b*) L. Lu, G. A. N. Gowda, N. Suryaprakash, C. L. Khetrapal and R. G. Weiss, *Liq. Cryst.*, 1998, **25**, 295–300.

5 D. W. Bruce, Y. Gao, J. N. Canongia Lopes, K. Shimizu and J. M. Slattery, *Chem. Eur. J.*, 2016, **22**, 16113–16123.

6 (*a*) S. Yazaki, M. Funahashi, J. Kagimoto, H. Ohno and T. Kato, *J. Am. Chem. Soc.*, 2010, **132**, 7702–7708; (*b*) S. Yazaki, M. Funahashi and T. Kato, *J. Am. Chem. Soc.*, 2008, **130**, 13206–13207.

7 E. Guillet, D. Imbert, R. Scopelliti and J.-C. G. Bünzli, *Chem. Mater.*, 2004, **16**, 4063–4070.

8 K. S. Egorova and V. P. Ananikov, *ChemSusChem*, 2014, **7**, 336–360.

9 Selected recent examples: J. Pernak, B. Legosz, F. Walkiewicz, T. Klejdysz, A. Borkowski and L. Chrzanowski, *RSC Adv.*, 2015, **5**, 65471–65480

10 J. Gravel and A. R. Schmitzer, *Org. Biomol. Chem.*, 2017, **15**, 1051–1071.

11 S. Klembt, S. Dreyer, M. Eckstein and U. Kragl, in *Ionic Liquids in Synthesis*, 2nd ed., ed. P. Wasserscheid and T. Welton, Wiley-VCH, Weinheim, 2008, Vol. 2, pp 641–662.

12 Q. Wang, D. Mao and Y. Luo, *Environ. Sci. Technol.*, 2015, **49**, 8731–8740.

13 D. Wang, C. Richter, A. Rühling, P. Drücker, D. Siegmund, N. Metzler-Nolte, F. Glorius and H.-J. Galla, *Chem. Eur. J.*, 2015, **21**, 15123–15126.

14 R. I. Benhamou, P. Shaul, I. M. Herzog and M. Fridman, *Angew. Chem., Int. Ed.*, 2015, **54**, 13617–13621.

15 (*a*) J. G. Hurdle, A. J. O'Neill, I. Chopra and R. E. Lee, *Nat. Rev. Microbiol.*, 2011, **9**, 62–75; (*b*) R. E. W. Hancock and H.-G. Sahl, *Nat. Biotechnol.*, 2006, **24**, 1551–1557.

16 K. S. Egorova, M. M. Seitkalieva, A. V. Posvyatenko and V. P. Ananikov, *Toxicol. Res.*, 2015, **4**, 152–159.

17 J. Martín, G. Crespo, V. González-Menéndez, G. Pérez-Moreno, P. Sánchez-Carrasco, I. Pérez-Victoria, L. M. Ruiz-Pérez, D. González-Pacanowska, F. Vicente, O. Genilloud, G. F. Bills and F. Reyes, *J. Nat. Prod.*, 2014, **77**, 2118–2123.

18 S. T. Reddy, K. P. Krovi and M. J. Swamy, *Cryst. Growth Des.*, 2014, **14**, 4944–4954.

19 D. Sivaramakrishna and M. J. Swamy, *Langmuir*, 2015, **31**, 9546–9556.

20 W. Dobbs, B. Heinrich, C. Bourgogne, B. Donnio, E. Terazzi, M.-E. Bonnet, F. Stock, P. Erbacher, A.-L. Bolcato-Bellemin and L. Douce, *J. Am. Chem. Soc.*, 2009, **131**, 13338–13346.

21 R. T. W. Huang, K. C. Peng, H. N. Shih, G. H. Lin, T. F. Chang, S. J. Hsu, T. S. T. Hsu and I. J. B. Lin, *Soft Matter*, 2011, **7**, 8392–8400.

22 M. M. Neidhardt, M. Wolfrum, S. Beardsworth, T. Wöhrle, W. Frey, A. Baro, C. Stubenrauch, F. Giesselmann and S. Laschat, *Chem. Eur. J.*, 2016, **22**, 16494–6504.

23 J. N. Israelachvili, D. J. Mitchell and B. W. Ninham, *J. Chem. Soc. Faraday Trans. 2*, 1976, **72**, 1525–1568.

24 C. Tschierske, *J. Mater. Chem.*, 1998, **8**, 1485–1508.

25 N. Joondan, S. Jhaumeer-Laulloo and P. Caumul, *Microbiol. Res.*, 2014, **169**, 675–685.

26 W. Kantlehner, E. Haug, W. W. Mergen, P. Speh, T. Maier, J. J. Kapassakalidis, H.-J. Bräuner and H. Hagen, *Liebigs Ann. Chem.*, 1984, 108–126.

27 X. Cheng, X. Bai, S. Jing, H. Ebert, M. Prehm and C. Tschierske, *Chem. Eur. J.*, 2010, **16**, 4588–4601.

28 (*a*) M. R. Imam, M. Peterca, U. Edlund, V. S. K. Balagurusamy and V. Percec, *J. Polym. Sci., Part A: Polym. Chem.*, 2009, **47**, 4165–4193; (*b*) B. M. Rosen, C. J. Wilson, D. A. Wilson, M. Peterca, M. R. Imam and V. Percec, *Chem. Rev.*, 2009, **109**, 6275–6540.

29 Software Avogadro, Version 1.1.1, for details see: M. D. Hanwell, D. E. Curtis, D. C. Lonie, T. Vandermeersch, E. Zurek and G. R. Hutchison, *J. Cheminf.*, 2012, **4**, 17.

30 S. Yazaki, Y. Kamikawa, M. Yoshio, A. Hamasaki, T. Mukai, H. Ohno and T. Kato, *Chem. Lett.*, 2008, **37**, 538–539.

31 (*a*) K. Fujimura, T. Ichikawa, M. Yoshio, T. Kato and H. Ohno, *Chem. Asian J.*, 2016, **11**, 520–526; (*b*) T. Ichikawa, K. Fujimura, M. Yoshio, T. Kato and H. Ohno, *Chem. Commun.*, 2013, **49**, 11746–11748.

32 M. Ishiyama, M. Shiga, K. Sasamoto, M. Mizoguchi and P. He, *Chem. Pharm. Bull.*, 1993, **41**, 1118–1122.

33 M. McLaughlin, M. J. Earle, M. A. Gîlea, B. F. Gilmore, S. P. Gorman and K. R. Seddon, *Green Chem.*, 2011, **13**, 2794–2800.

34 A. Paternò, F. D'Anna, G. Musumarra, R. Noto and S. Scirè, *RSC Adv.*, 2014, **4**, 23985–24000.

35 K. R. Gee, K. A. Brown, W-N. U. Chen, J. Bishop-Stewart, D. Gray and I. Johnson, *Cell Calcium*, 2000, **27**, 97–106.

36 S. Vylkova, X. S. Li, J. C. Berner and M. Edgerton, *Antimicrob. Agents Chemother.*, 2006, **50**, 324–331.

37 (*a*) H. Utsumi, K. Kiyoshige, S. Shimbara and A. Hamada, *Environmental. Toxicol. Water Qual.*, 1994, **9**, 333–339; (*b*) S. A. Prestwich, H. Miyazaki and T. B. Bolton, *British J. Pharmacol.*, 1995, **115**, 147–157.

38 A. J. Ryan, N. M. Gray, P. N. Lowe and C.-W. Chung, *J. Med. Chem.*, 2003, **46**, 3448–3451.

39 N. Amdursky and M. M. Stevens, *ChemPhysChem*, 2015, 2768–2774.

40 (a) K. Jodko-Piorecka and G. Litwinienko, *ACS Chem. Neurosci.*, 2013, **4**, 1114–1122; (b) K. Jodko-Piorecka and G. Litwinienko, *Free Radical Biol. Med.*, 2015, **83**, 1–11.

41 A. W. Thomas, C. Catania, L. E. Garner and G. C. Bazan, *Chem. Comm.*, 2015, **51**, 9294–9297.

42 T. Murayama, T. Masuda, S. Afonin, K. Kawano, T. Takatani-Nakase, H. Ida, Y. Takahashi, T. Fukuma, A. S. Ulrich and S. Futaki, *Angew. Chem., Int. Ed.*, 2017, **56**, 7644–7647.

43 W. F. Walkenhorst, *Biochim. Biophys. Acta*, 2016, **1858**, 926–935.

44 R. M. Epand, C. Walker, R. F. Epand and N. A. Magarvey, *Biochim. Biophys. Acta*, 2016, **1858**, 980–987.

45 B. Wang, B. Pachaiyappan, J. D. Gruber, M. G. Schmidt, Y.-M. Zhang and P. M. Woster, *J. Med. Chem.*, 2016, **59**, 3140–3151.